Magnetic structures of quaternary intermetallic borocarbides RCo_2B_2C (R = Dy, Ho, Er)

2009 J. Phys.: Condens. Matter 21 436006

(http://iopscience.iop.org/0953-8984/21/43/436006)

J. Phys.: Condens. Matter **21** (2009) 436006 (7pp) doi:10.1088/0953-8984/21/43/436006

Magnetic structures of quaternary intermetallic borocarbides RCo_2B_2C (R = Dy, Ho, Er)

M ElMassalami[1], R Moreno[1], H Takeya[2], B Ouladdiaf[3], J W Lynn[4] and R S Freitas[5]

[1] Instituto de Fisica, Universidade Federal do Rio de Janeiro, Caixa Postal 68528, 21945-970 Rio de Janeiro, Brazil
[2] National Institute for Materials Science, 1-2-1 Sengen, Tsukuba, Ibaraki 305-0047, Japan
[3] Institut Laue-Langevin, BP 156, 38042 Grenoble Cedex 9, France
[4] NIST Center for Neutron Research, National Institute of Standards and Technology, Gaithersburg, MD 20899-6102, USA
[5] Instituto de Física, Universidade de São Paulo, Rua do Matão 187 Travessa R, Cidade Universitária, 05315-970 Sao Paulo, SP, Brazil

Received 24 March 2009, in final form 31 August 2009
Published 8 October 2009
Online at stacks.iop.org/JPhysCM/21/436006

Abstract
The magnetic structures of the title compounds have been studied by neutron diffraction. In contrast to the isomorphous RNi_2B_2C compounds, wherein a variety of exotic incommensurate modulated structures has been observed, the magnetic structure of $ErCo_2B_2C$ is found to be a collinear antiferromagnet with $k = (\frac{1}{2}, 0, \frac{1}{2})$ while those of $HoCo_2B_2C$ and $DyCo_2B_2C$ are observed to be simple ferromagnets. For all studied compounds, the moments are found to be confined within the basal plane and their magnitudes are comparable to the values obtained from the low-temperature isothermal magnetization measurements. The absence of modulated magnetic structures in the RCo_2B_2C series (for $ErCo_2B_2C$, verified down to 50 mK) is attributed to the quenching of the Fermi surface nesting features.

(Some figures in this article are in colour only in the electronic version)

1. Introduction

One of the most striking features of the magnetism of the RNi_2B_2C series is the manifestation of a variety of incommensurate modulated antiferromagnetic-like structures, some of which coexist with a superconducting ground state [1–3]. There are three different types of modulations: $\vec{k}_1 \simeq (0.55, 0, 0)$ as in R = Gd, Tb, Ho ($T_N < T < 6.5$ K), Er; $\vec{k}_2 \simeq (0.093, 0.093, 0)$ as in R = Tm; and $\vec{k}_3 \simeq (0, 0, 0.91)$ as in R = Ho ($T_N < T < 8$ K). In addition, there are two commensurate antiferromagnetic (AFM) structures having $\vec{k}_4 = (0, 0, 1)$ as in R = Pr, Dy, Ho ($T \leqslant T_N$), and $\vec{k}_5 = (0.5, 0, 0.5)$ as in R = Nd. For the case of R = Ho, the $\vec{k}_1$, $\vec{k}_3$, and $\vec{k}_4$ modes coexist within a narrow range of temperature [2]. The manifestation of such a variety of wavevectors is not uncommon in intermetallic magnets wherein the magnetic couplings are mediated by the indirect Ruderman–Kittel–Kasuya–Yosida (RKKY) interactions [4]: indeed, for the particular case of RNi_2B_2C, the presence of these RKKY interactions is evidenced as a de Gennes scaling of both the superconducting and magnetic transition temperatures [1, 3].

As is generally the case, the type of the magnetic structure for the rare-earth moments in RNi_2B_2C is determined by the competition between these RKKY interactions, the crystalline electric field (CEF) forces, and the classic dipolar interactions [5–7]. The RKKY interactions (and thus the magnetic structure) of these borocarbides depend partially on the spatial separation of their R^{3+} ions as well as on their electronic band structures. The importance of the latter is highlighted by the observation that the $\vec{k}_1$ mode is related to the electronic nesting features that give rise to a peak in the generalized susceptibility [8].

It is worth mentioning that the manifestation of a variety of wavevectors in the RT_2B_2C family is not forbidden by group theory arguments [9–11]. In fact, for these tetragonal borocarbides ($I4/mmm$), where the magnetic moments reside

at the Wyckoff site 2a, Wills *et al* [9] showed that there are 15 possible wavevectors; each (or a superposition) of them can be used to describe a distinct magnetic structure (see table 3 of [9]). As mentioned above, the stabilization of a specific structure depends critically on the energy balance among the CEF, dipolar, and exchange interactions. It is interesting to note that one of the possible magnetic states that are predicted by this representational analysis is ferromagnetic (FM): such an FM state has not been observed in RNi_2B_2C, but, as shown in a previous report [12] as well as in this work, an FM structure is manifested in a number of RCo_2B_2C compounds.

Based on electronic band structures of the RT_2B_2C (R = Lu, Y; T = Ni, Co) compounds [13, 14], their Sommerfeld specific-heat coefficients are almost equal. Furthermore, for the magnetic isomorphs, each Co- and Ni-based pair has almost equal lattice parameters and similar R^{3+} single-ion crystalline electric field properties [15]. Then it is expected that the multi-k-vector character should also be manifested in the isomorphous RCo_2B_2C series. Contrary to this expectation, the reported magnetic structures of RCo_2B_2C (R = Tb [12], Tm [16]) are found to be ferromagnetic, in distinct contrast to the modulated spin configuration of the Ni-based isomorphs. As this work shows, the magnetic structures of RCo_2B_2C (R = Dy, Ho, Er) are also different from their Ni-based isomorphs: while the structures of R = Dy, Ho are ferromagnetic, that of R = Er is commensurate antiferromagnetic.

The difference in the magnetic structure of these isomorphous RT_2B_2C (T = Ni, Co) series is attributed to the following: electronic band structure calculations [13, 14, 17–19] demonstrated that the density of states at the Fermi level, $N(E_F)$, of both series receives appreciable contribution from the 3d orbitals of the transition-metal atoms. Since the electronic properties of the RT_2B_2C family can be reasonably well described in terms of the rigid band model, the substitution of Co atoms (which have a lower number of 3d electrons) induces a downward shift in E_F but with a new $N(E_F)$, which is almost equal to that of RNi_2B_2C (compare figures 1 and 4 of [13]). Such a shift entails a difference in the generalized susceptibilities and thus a difference in the character of the magnetic ground state.

2. Experiment

99.5% ^{11}B enriched polycrystals of RCo_2B_2C were prepared by the conventional arc-melt method. Powder neutron diffraction measurements on as-prepared samples were carried out at the Institut Laue–Langevin (ILL), France (D1A $\lambda = 1.91$ Å, 1.3 K $\leqslant T \leqslant$ 30 K) and the National Institute of Standards and Technology (NIST), USA (BT-9 triple-axis instrument with a pyrolytic graphite monochromator and filter, $\lambda = 2.359$ Å, 0.05 K $\leqslant T \leqslant$ 8.0 K, and BT-1 high resolution powder diffractometer with $\lambda = 2.0787$ Å). Due to experimental difficulties, the neutron diffractograms within the mK range were measured only for $ErCo_2B_2C$ (section 3.1). Similarly, detailed temperature dependent diffractograms were collected only for $HoCo_2B_2C$ (section 3.2), though we were not able to study its diffractograms below 1.5 K.

Taking into account the well known properties of the crystal structures of borocarbides [2, 20] together with the successful indexation of the magnetic structures of the title compounds, the Rietveld powder analysis, using the FULLPROF package for ILL data and GSAS for the NIST data, was employed to refine the parameters of both crystallographic and magnetic structures. As we mentioned in an earlier report [12], the Co atoms are not polarized (if there were any moment it would be less than 0.25 μ_B): accordingly, magnetic moments are admitted only on the R^{3+} sites. The results of refining the main parameters (such as lattice unit cell, magnetic unit cell, thermal and occupation parameters) were satisfactory, yielding low χ^2 (in the range of 2), R_P (4–8), and R_{WP} (4–9). The obtained values of the refined occupation and thermal parameters as well as the z-parameter of the B atoms were found to be the same (within the experimental errors) as the ones reported for the corresponding RNi_2B_2C isomorphs (see table 1 of Lynn *et al* [2]). In some of the refinements, no absorption corrections were taken into account; as a consequence, the obtained magnetic moments were found to be lower than the values deduced from the isothermal magnetization measurements (this is more evident in the case of $DyCo_2B_2C$).

Magnetization $M(T, H)$ measurements (sections 3.2 and 3.3) were carried out on a vibrating-sample magnetometer, which was operated within the range (0.5 K $< T <$ 30 K, $H <$ 17 T). During the analysis of the magnetization isotherms, we drew a distinction between the so-called spontaneous moment, $\mu_{(H\to 0)}$, and the saturation moment, $\mu_{(\frac{1}{H}\to 0)}$. In contrast to most other compounds, wherein the difference between these limit moments is not appreciable enough to warrant such a distinction, the magnetization isotherms of some of the RCo_2B_2C compounds (particularly R = Dy, Er, Tm) do not show magnetic saturation even in magnetic fields of 15 T: this feature—analyzed as a high-field magnetic susceptibility, most evident in the single-crystal magnetization of $TbCo_2B_2C$ [12]—is most probably due to a weak electronic polarization or a field-induced perturbation of the CEF interactions. Finally, it is expected that, for each compound measured at a specific temperature, the value of its magnetic moment determined from the powder zero-field magnetic diffractogram is comparable to its spontaneous magnetic moment determined from the magnetization isotherm.

3. Results

3.1. $ErCo_2B_2C$

Based on earlier zero-field ac susceptibility and specific-heat results [15], the magnetic order of $ErCo_2B_2C$ sets in at $T_N = 4.0(1)$ K. Indeed, below T_N the diffractograms of $ErCo_2B_2C$ (figure 1) show additional intense magnetic-origin Bragg peaks, which can be indexed on the basis of the magnetic structure shown in figure 2: a commensurate, collinear, antiferromagnetic structure with the moments being coupled antiferromagnetically along both a and c axes and ferromagnetically along the b axis, i.e. $\vec{k} = (\frac{1}{2}\ 0\ \frac{1}{2})$. It is worth mentioning that this AFM character is also manifested in the magnetization isotherm of figure 3.

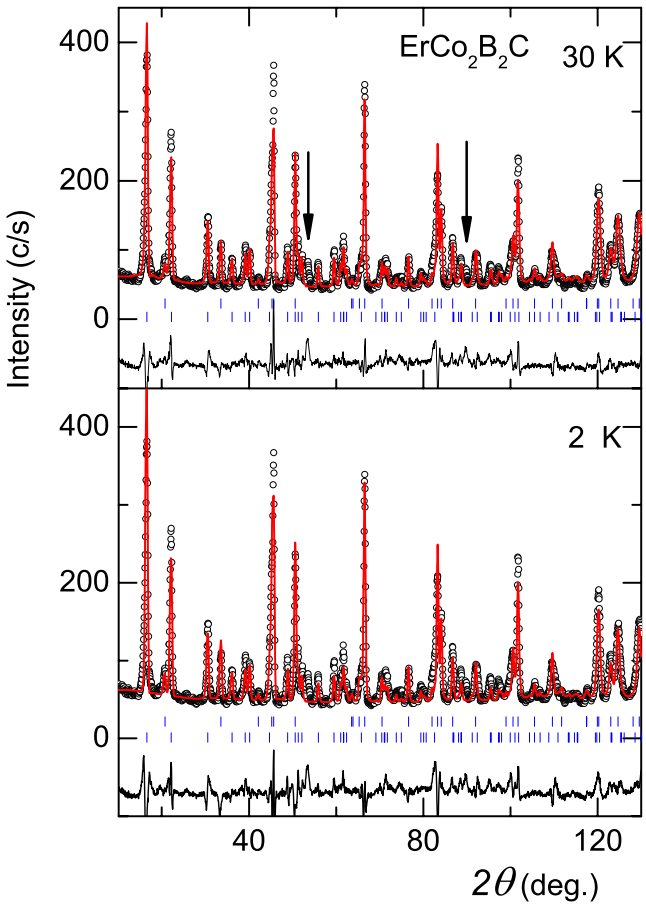

Figure 1. Representative neutron diffractograms of $ErCo_2B_2C$ measured at 2 K (low panel) and 30 K (top panel). Symbols, solid line, and short vertical bars represent, respectively, measured intensities, calculated intensities based on Rietveld refinement, and positions of the Bragg reflections. The differences between the measured and calculated intensities are shown as difference curves. For the reliability factors of the refinements see section 2. The vertical arrows indicate the positions of the strongest contaminating peaks.

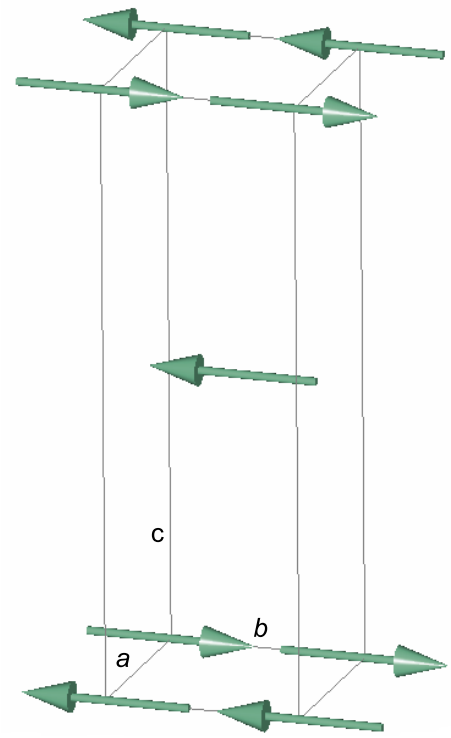

Figure 2. The commensurate, collinear, antiferromagnetic structure of $ErCo_2B_2C$. The moments are coupled antiferromagnetically along both the *a* and *c* axes and ferromagnetically along the *b* axis (see the text).

Evidently the above-mentioned AFM structure requires that the *a*- and *b*-parameters be distinct even though the crystal structure of the paramagnetic phase is tetragonal. In fact, a similar distinction in the basal plane parameters was already reported for the case of the $ErNi_2B_2C$ [21–23] and $NdNi_2B_2C$ [2] isomorphs: $NdNi_2B_2C$, in particular, orders antiferromagnetically with the same $\vec{k} = (\frac{1}{2}\ 0\ \frac{1}{2})$. In these compounds, such a distinction is attributed to an orthorhombic distortion of the tetragonal cell, which is driven by magnetoelastic forces. In the present measurements this distortion is too small to be detected, as was the case for the initial neutron powder work on RNi_2B_2C systems [2].

Based on the refinement of the powder diffractograms (figure 1), the Er^{3+} moment is found to be confined within the basal plane and reaches 6.8(2) μ_B at 2.0 K. This value is higher than the spontaneous moment ($\mu_{(H\to 0)} = 5.9 \pm 0.2\ \mu_B$) but is in agreement with the saturation moment ($\mu_{(\frac{1}{H}\to 0)} = 7.1 \pm 0.1\ \mu_B$), both obtained from the isothermal magnetization measured at 1.30(5) K (figure 3). Moreover, it compares favorably with the value reported for $ErNi_2B_2C$ ($7.2 \pm 0.1\ \mu_B$) [2], suggesting a similarity in their single-ion properties; however, there are important differences: the Co-based isomorph does not superconduct and does not manifest an incommensurate magnetic structure; rather, it orders into a collinear AFM structure at a critical temperature which is 40% lower than that of the Ni-based isomorph.

It was reported earlier that both the specific heat and ac susceptibility curves of an $ErCo_2B_2C$ sample exhibit a magnetic anomaly at $T_M = 0.37(2)$ K [15]. For the purpose of investigating the origin of this magnetic T_M event, we collected neutron diffractograms at various temperatures: 50 mK (well below T_M), 700 mK (just above T_M but well below T_N), and 8 K (above T_N). As can be seen in figure 4, there are no additional magnetic peaks (or any other features) that can be associated with this anomaly. In fact, the inset of figure 4 indicates that the magnetic patterns at 700 and 50 mK are identical. As there is no change in the diffractograms when the temperature is cooled through the reported T_M, it is concluded that the reported anomalous transition at T_M may correspond to an ordered moment that is too small to be detected in powder diffraction, or it does not correspond to a new long-range ordered state. We also cannot rule out that it is a sample dependent effect, which would imply that it is not fundamental to the Er-sublattice magnetic order.

3.2. *$HoCo_2B_2C$*

The diffractograms of $HoCo_2B_2C$ (figure 5) show that there are no additional satellite peaks when the sample is cooled below

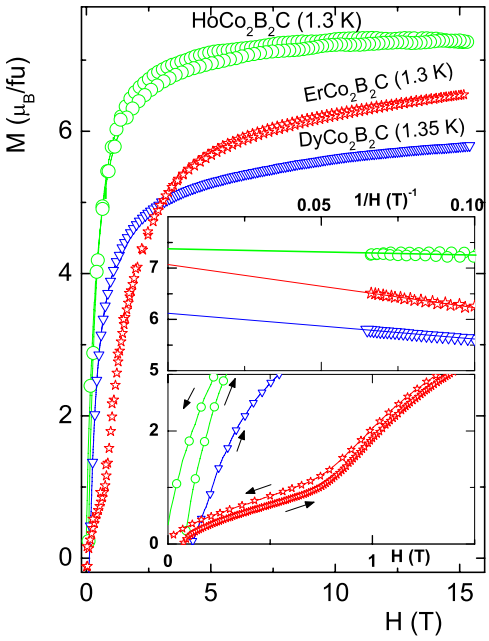

Figure 3. Magnetization isotherms of RCo_2B_2C (R = Dy, Ho, Er) measured at the indicated temperatures. The lower inset shows an expansion of the low-field region of the forced magnetization: while $M(T, H)$ of R = Dy, Ho is typical of a forced domain movement of an FM state, that of R = Er is characteristic of a field-induced spin-flop anomaly of an AFM structure. The upper inset gives the saturated magnetization when $H \to \infty$ ($\frac{1}{H} \to 0$): for R = Dy and Er, no saturation is attained even for a field of 15 T. Similar high-field magnetization features were observed in $TbCo_2B_2C$ (see figure 2 of [12]) and $TmCo_2B_2C$ (see figure 6 of [16]).

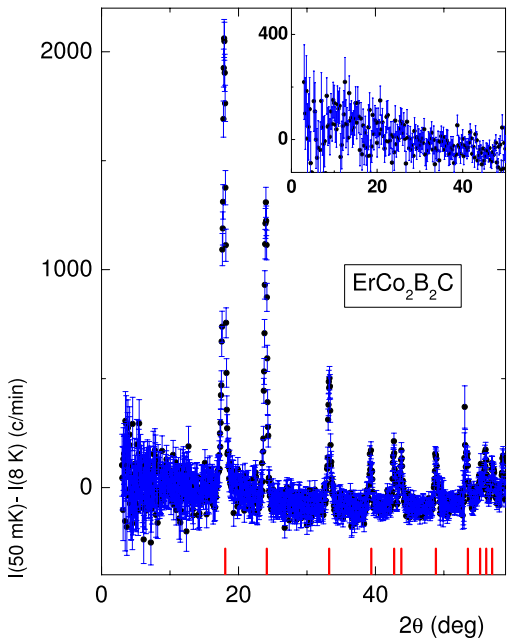

Figure 4. Low-temperature magnetic diffractogram of $ErCo_2B_2C$ obtained after subtracting the nuclear contributions (diffractogram at 8 K) from the one at 50 mK; the solid vertical bars index the magnetic pattern. The inset shows the difference pattern obtained after subtracting the diffractogram at 700 mK from that of 50 mK: evidently there is no change in the magnetic structure (see the text). The indicated uncertainties are statistical in nature and represent one standard deviation.

$T_C = 5.4(2)$ K; instead, there is a considerable enhancement in the intensities of the fundamental Bragg peaks. The resulting magnetic pattern is easily indexed on the basis of an FM unit cell which is of the same dimensions as the crystalline one. The Rietveld analysis (see figure 6) confirms the conclusions drawn from the magnetic indexing: an FM structure with the moments lying within the basal plane. The thermal evolution of the Ho^{3+} moments (figure 7) shows a tendency towards saturation to a moment of 7.2(2) μ_B. This is in excellent agreement with the spontaneous moment ($\mu_{(H\to 0)} = 7.3 \pm 0.1\ \mu_B$) but slightly lower than the saturation moment ($\mu_{(\frac{1}{H}\to 0)} = 7.4 \pm 0.1)\ \mu_B$, both obtained from the isothermal magnetization measured at 1.30(5) K (see figure 3). Furthermore, figure 7 indicates that the intensity monotonically decreases as T_C is being approached from below, and that it decreases almost linearly above T_C such that it becomes zero at 6.7 K. The presence of magnetic intensity well above T_C (attributed to short-range order) has already been observed in the specific heat and susceptibility of $HoCo_2B_2C$ [15]. Similar short-range features were observed in the neutron diffraction studies on the $HoNi_2B_2C$ isomorph [2].

In stark contrast with the exotic features of the low-temperature magnetic phase diagram of $HoNi_2B_2C$ [1, 3], the above results demonstrate that $HoCo_2B_2C$ orders into a simple FM state and that within the studied temperature range ($1.5\ K < T < T_C$) there are no manifestations of additional zero-field order-to-order magnetic transformations. In an earlier work, we reported that $HoCo_2B_2C$ undergoes a zero-field, order-to-order magnetic transition at $T_m = 1.5$ K [15]. Unfortunately, during the present work, we were unable to collect diffractograms below 1.5 K. Nonetheless, considering the evidence collected on $ErCo_2B_2C$ (see section 3.1) and $TbCo_2B_2C$ [12], we are inclined to attribute such a transition at T_m to a minor contaminating magnetic phase.

3.3. $DyCo_2B_2C$

Figure 8 shows the thermal evolution of the diffraction pattern of $DyCo_2B_2C$ when cooled through the magnetic transition temperature ($T_C = 8.0(2)$ K). On subtracting the paramagnetic diffractogram at 10 K from the one at 1.4 K, we obtain the magnetic diffraction pattern shown in the upper panel of figure 8. This pattern can be indexed on the basis of an FM cell having the same dimensions as those of the crystalline one. Assuming such a ferromagnetic unit cell and the orientation of the moments to be along the (110) axis, we carried out a Rietveld refinement on the diffractograms of figure 8. The refined patterns are shown in figure 9 and the obtained zero-field magnetic moment of Dy at 1.3 K is 5.2(2) μ_B. Based on the analysis of powder, isothermal magnetization measurements at 1.35(5) K (see figure 3), this moment value is similar to the spontaneous moment ($\mu_{(H\to 0)} = 5.3 \pm 0.2\ \mu_B$) but lower than the saturation moment ($\mu_{(\frac{1}{H}\to 0)} = 6.2 \pm 0.1\ \mu_B$). It is noted that all these moment values are lower that the one reported for the $DyNi_2B_2C$ isomorph (see table 1).

Table 1. Some structural and magnetic parameters of the isomorphous RNi_2B_2C and RCo_2B_2C series (R = Tm, Er, Ho, Dy, Tb). The room-temperature cell dimensions of RNi_2B_2C (RCo_2B_2C) are determined from neutron [24] (x-ray [15, 16]) diffraction. The magnetic properties of RNi_2B_2C are taken from [24, 25] while those of $TbCo_2B_2C$ and $TmCo_2B_2C$ are taken, respectively, from [12] and [16]. The symbols have their usual meanings. $|\vec{\mu}|$ refers to the value obtained from the neutron diffraction analysis.

R	Tm		Er		Ho		Dy		Tb	
M	Co	Ni	Co	Ni	Co	Ni	Co	Ni	Co	Ni
a (Å)	3.473	3.4866	3.4844	3.5019	3.4997	3.5177	3.5099	3.534 20	3.5246	3.5536
c (Å)	10.647	10.607	10.5902	10.5580	10.544 65	10.5278	10.5268	10.4878	10.5176	10.4352
T_{crit} (K)	0.8	1.53	4.0	6.8	5.4	5.0	8.0	10.6	6.3	15.0
Mode	FM	TSW	AFM	TSW	FM	AF	FM	AF	FM	LSW
$\vec{k}$	(0, 0, 0)	(0.093, 0.093, 0)	$(\frac{1}{2}, 0, \frac{1}{2})$	(0.553, 0, 0)	(0, 0, 0)	(0, 0, 1)	(0, 0, 0)	(0, 0, 1)	(0, 0, 0)	(0.555, 0, 0)
$\|\vec{\mu}\|$	∼1	3.8	6.8(2)	7.2	7.2(2)	8.6	> 5.2(2)	8.5	7.6	7.8
Easy axis	(0, 0, 1)	(0, 0, 1)	(0, 1, 0)	(0, 1, 0)	(1, 1, 0)	(1, 1, 0)	(1, 1, 0)	(1, 1, 0)	(1, 0, 0)	(1, 0, 0)

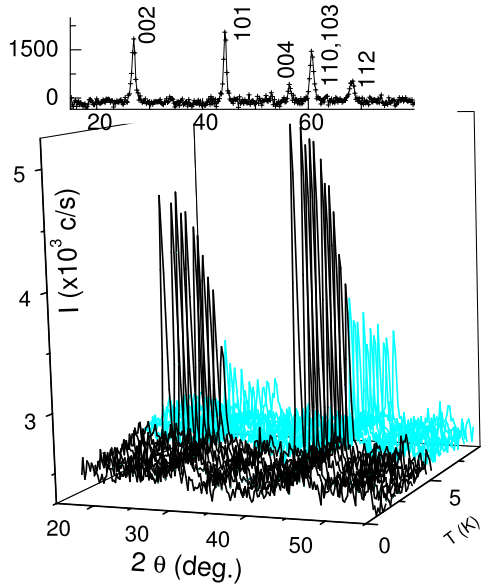

Figure 5. Lower panel: three-dimensional plot of representative powder diffractograms of $HoCo_2B_2C$. The intensities are measured over a wide range of scattering angle (here, for clarity, they are shown only up to 55°) and at various temperatures. The enhancement of the intensities at the positions of the nuclear Bragg peaks is clearly manifested below T_C. The fact that there are no additional magnetic peaks and that the Ho site is at the 4a site indicates that the magnetic arrangement must be due to an onset of ferromagnetism (see text). This is confirmed in the upper panel, which shows the difference plot of I (1.5 K) − I (10 K) together with the Bragg peak identifications.

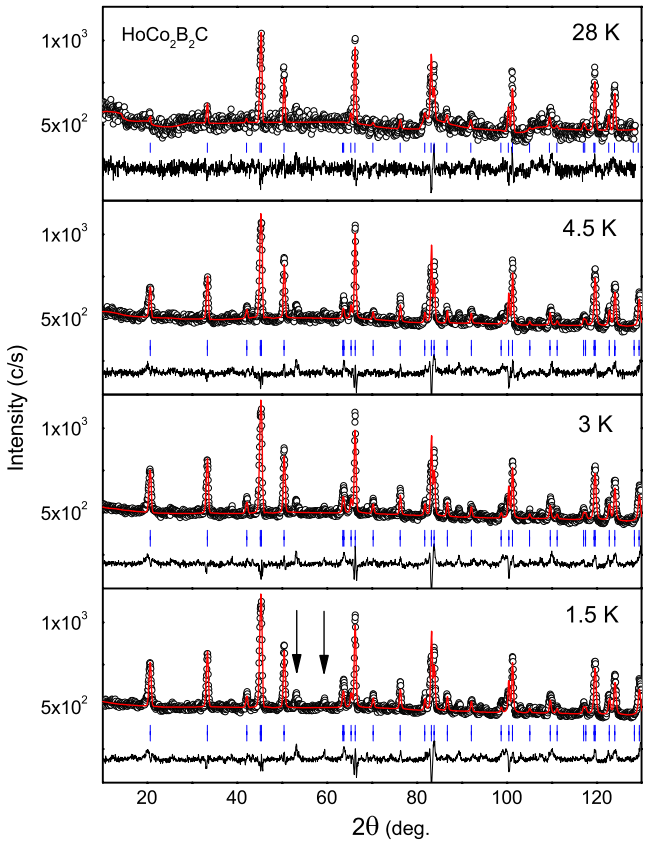

Figure 6. Rietveld refinement of representative powder diffractograms of $HoCo_2B_2C$. Symbols, solid line, and short vertical bars represent, respectively, observed intensities, model calculation, and positions of the Bragg reflections. The difference plots are shown in the lower part of each panel. For the reliability factors of the refinements see section 2. The vertical arrows indicate the positions of the strongest contaminating peaks.

4. Discussion and conclusion

As mentioned above, the crystalline electric field environment around the R^{3+} site in the RCo_2B_2C series is expected to be the same as the one observed in the isomorphous RNi_2B_2C series. Consequently, the single-ion properties of R^{3+} should be similar: specifically, the ordered moment direction in the sequence of pairs DyT_2B_2C, HoT_2B_2C, and ErT_2B_2C (T = Co, Ni) should be similar (see table 1). This working assumption is particularly helpful since the zero-field powder neutron diffraction technique is only able to identify the deviation of the moment with respect to the unique (tetragonal) axis. In the present case, it can identify that the moments are within the *ab*-plane, but not the easy axis within the plane. Then, based on this similarity of the CEF properties, the easy axis of both R = Dy, Ho is taken to be (1, 1, 0) while that of R = Er is taken to be along the (0, 1, 0) direction. It is reassuring that these arguments have been experimentally verified for the case of the $TbCo_2B_2C$ single crystal [12].

A comparison of the magnetic phase diagrams of the RCo_2B_2C and RNi_2B_2C series shows that there are four distinct differences among these isomorphs.

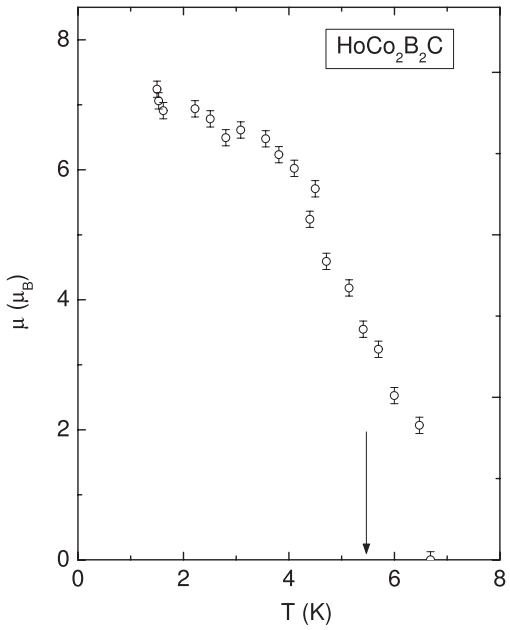

Figure 7. Thermal evolution of the ordered magnetic moment for $HoCo_2B_2C$ as obtained from the neutron diffraction refinements of figure 6. T_C is indicated by the vertical arrow.

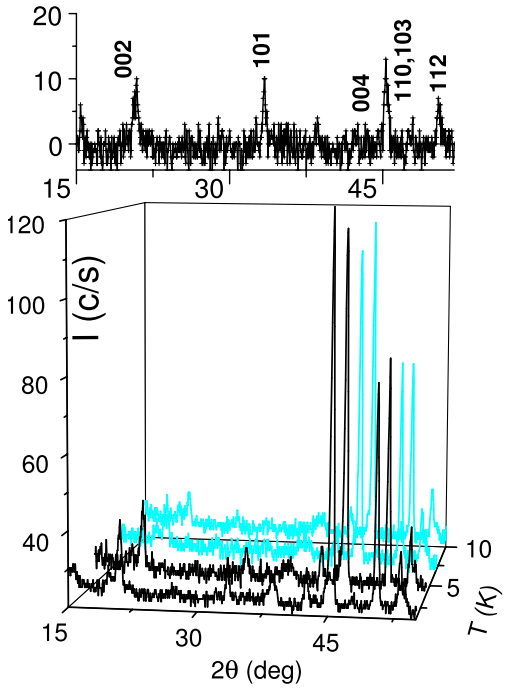

Figure 8. Lower panel: representative diffractograms of $DyCo_2B_2C$ measured at 1.4, 4, 7, and 10 K. The upper panel shows the difference plot (after subtracting the pattern at 10 K from the one at 1.4 K): the pattern is indexed based on a ferromagnetic structure.

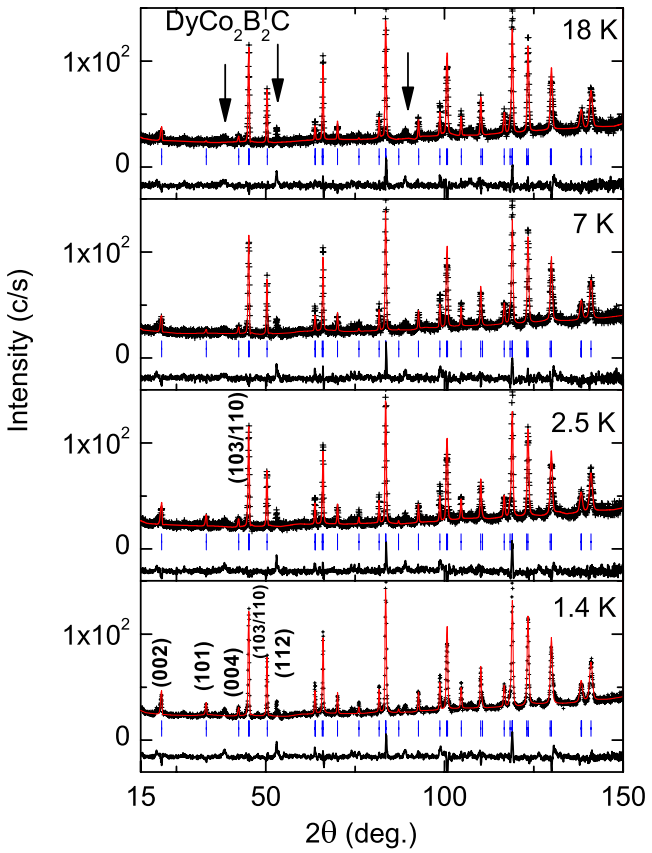

Figure 9. Refinements of representative diffractograms of $DyCo_2B_2C$. Except for the weak impurity peaks (denoted by short vertical arrows), the measured intensities (symbols) are well accounted for by the calculated profile (solid lines) based on the following crystalline and magnetic structures. The difference plots are given in the lower part of each panel. For the reliability factors of the refinements see section 2.

First, the magnetic transition temperatures of RCo_2B_2C are lower and do not follow a de Gennes scaling. In an earlier report [15], we illustrated the decisive influence of the CEF effect on the variation of the transition points, T_{crit}, by quoting the work of Noakes and Shenoy [26], which showed that T_{crit} can be enhanced much more than predicted by the de Gennes analysis if the second-order crystal-field parameter B_2^0 is large and positive:

$$T_{crit}\alpha\xi\left(\sum_{J_z} J_z^2 \exp(-3B_2^0 J_z^2/T_{crit})\right) \times \left(J(J+1)\sum_{J_z}\exp(-3B_2^0 J_z^2/T_{crit})\right)^{-1}.$$

This relation shows that the de Gennes scaling is not expected to be obeyed since B_2^0 is not a smooth function of ξ and that, moreover, T_{crit} of the individual RT_2B_2C isomorphs would be different if the B_2^0 were not the same: this case is evident in, say, $TbCo_2B_2C$ ($T_C = 6.3$ K, $B_2^0 = 0.8$ K) and $TbNi_2B_2C$ ($T_N = 15$ K, $B_2^0 = 1.2$ K).

Second, the values of the ordered magnetic moments of RCo_2B_2C are smaller than those of RNi_2B_2C isomorphs and both are lower than the corresponding free ion value. This reduction is also attributed to crystalline electric field effects: the variation of B_2^0 between the $TbCo_2B_2C$ and $TbNi_2B_2C$ isomorphs supports this viewpoint.

Third, the observation that the studied RCo_2B_2C compounds do not exhibit any type of incommensurate

modulated states is an indication that those nesting features that are responsible for the modulated mode in the RNi_2B_2C isomorphs [8] must have been quenched in the Co-based compounds. Indeed, the details of the electronic structure of YCo_2B_2C and YNi_2B_2C are quite different [13, 14].

Fourth, there is no evidence of any metamagnetic field-induced transitions (except for the spin-flip transition of R = Er) in the magnetization isotherms shown in figure 3 for R = Dy, Ho, Er (for $TbCo_2B_2C$ see figure 2 of [12], while for $TmCo_2B_2C$ see figure 6 of [16]). No field-induced metamagnetic transitions are expected in commensurate FM structures.

The four above-mentioned observations highlight the delicate balance between the exchange, crystalline, and dipolar interactions in establishing the exotic magnetic phase diagrams of these borocarbides. It is worth mentioning that the incommensurate modulation (third property) and the (field-induced) metamagnetic transformations (fourth property) do not always show up in the same compound: as an example, $GdNi_2B_2C$ (wherein there are exchange and dipolar forces but no CEF interaction) does manifest a modulated state but no cascade of field-induced metamagnetic transformations [27].

The FM structure of RCo_2B_2C (e.g. R = Tb, Dy, Ho, Tm) is expected to generate a large internal molecular field at the Co site. Then, if this internal field exceeds a certain critical value, the Co sublattice could be spontaneously polarized [28–31]. We were particularly interested in the prospect of the Co sublattice being spontaneously polarized since this scenario was thought to support our earlier report of a second metamagnetic transformation (the T_M boundary) in the magnetic phase diagram of RCo_2B_2C [15]. It happened that the neutron diffractograms of the R = Dy, Ho, Er compounds as well as those of $TbCo_2B_2C$ [12] do not show any intrinsic order-to-order transformation of the rare-earth sublattice. Furthermore, this T_M transition is not always manifested in the recent thermodynamical measurements on $TbCo_2B_2C$ [12]. Consequently, it is inferred that there is no spontaneous polarization of the Co sublattice: if there is any it must be sample dependent.

In conclusion, this work has reported the magnetic structures as well as the magnetic phase diagrams of the above-mentioned RCo_2B_2C compounds and showed that their magnetic states are distinctly different from those of the corresponding Ni-based isomorphs. These findings should certainly contribute to our understanding of the magnetism and superconductivity and their interplay in the borocarbide series.

Acknowledgments

We acknowledge the partial financial support from the Brazilian agencies CNPq (485058/2006-5), Faperj (E-26/171.343/2005), and FAPESP (2008/00457-2).

References

[1] Müller K-H and Narozhnyi V N 2001 *Rep. Prog. Phys.* **64** 943
[2] Lynn J W, Skanthakumar S, Huang Q, Sinha S K, Hossain Z, Gupta L C, Nagarajan R and Godart C 1997 *Phys. Rev.* B **55** 6584
[3] Canfield P C, Gammel P L and Bishop D J 1998 *Phys. Today* **51** 40
[4] Coqblin B 1977 *The Electronic Structure of Rare-Earth Metals and Aloys: The Magnetic Heavy Rare-Earth* (New York: Acdemic)
[5] Kalatsky V A and Pokrovsky V L 1998 *Phys. Rev.* B **57** 5485
[6] Amici A and Thalmeier P 1998 *Phys. Rev.* B **57** 10684
[7] Jensen J 2002 *Phys. Rev.* B **65** 140514(R)
[8] Rhee J Y, Wang X and Harmon B N 1995 *Phys. Rev.* B **51** 15585
[9] Wills A S, Detlefs C and Canfield P C 2003 *Phil. Mag.* **83** 1227
[10] Ballou R and Ouladdiaf B 2006 *Neutron Scattering from Magnetic Materials* ed T Chatterji (Amsterdam: Elsevier) chapter 3, p 93
[11] Izyumov Y A, Naish V E and Ozerov R P 1991 *Neutron Diffraction of Magnetic Materials* (New York: Consultants Bureau)
[12] ElMassalami M, Moreno R, Saeed R M, Chaves F A B, Chaves C M, Rapp R E, Takeya H, Ouladdiaf B and Amara M 2009 *J. Phys.: Condens. Matter* **21** 216006
[13] Coehoorn R 1994 *Physica* C **228** 331
[14] Ravindran P, Johansson B and Eriksson O 1998 *Phys. Rev.* B **58** 3381
[15] ElMassalami M, DaCosta M S, Rapp R E and Chaves F A B 2000 *Phys. Rev.* B **62** 8942
[16] ElMassalami M, Rapp R E, Chaves F A B, Moreno R, Takeya H, Ouladdiaf B, Lynn J W, Huang Q, Freitas R S and Oliveria N F Jr 2009 *J. Phys.: Condens. Matter* **21** 046007
[17] Pickett W E and Singh D J 1994 *Phys. Rev. Lett.* **72** 3702
[18] Matthias L F 1994 *Phys. Rev.* B **49** 13279
[19] Lee J I, Zhao T S, Kim I G, Min B I and Youn S J 1994 *Phys. Rev.* B **50** 4030
[20] Siegrist T, Cava R, Krajewski J J and Peck W F 1994 *J. Alloys Compounds* **216** 135
[21] Doerr M, Rotter M, El Massalami M, Sinning S, Takeya H and Loewenhaupt M 2002 *J. Phys.: Condens. Matter* **14** 5609
[22] Detlefs C, Islam A H M Z, Gu T, Goldman A I, Stassis C, Canfield P C, Hill J P and Vogt T 1997 *Phys. Rev.* B **56** 7843
[23] Detlefs C, Abernathy D L, Grubel G and Canfield P C 1999 *Europhys. Lett.* **47** 352
[24] Lynn J W, Huang Q, Sinha S K, Hossain Z, Gupta L C, Nagarajan R and Godart C 1996 *J. Appl. Phys.* **79** 5857
[25] Chang L J, Tomy C V, Paul D M and Ritter C 1996 *Phys. Rev.* B **54** 9031
[26] Noakes D R and Shenoy G K 1982 *Phys. Lett.* A **91** 35
[27] El Massalami M, Takeya H, Hirata K, Amara M, Galera R-M and Schmitt D 2003 *Phys. Rev.* B **67** 144421
[28] Bloch D and Lemaire R 1970 *Phys. Rev.* B **2** 2648
[29] Bloch D, Edwards D M, Shimizu M and Voiron J 1975 *J. Phys. F: Met. Phys.* **5** 1217
[30] Cyrot M and Lavagna M 1979 *J. Phys. D: Appl. Phys.* **40** 763
[31] Cyrot M, Gignoux D, Givourd F and Lavagna M 1979 *J. Phys. D: Appl. Phys.* **40** C5